frontiers | Frontiers in Quantum Science and Technology

TYPE Original Research
PUBLISHED 19 June 2025
DOI 10.3389/frqst.2025.1535581

EDITED BY
Jorge Yago Malo,
University of Pisa, Italy

REVIEWED BY
Pietro Lombardi,
National Research Council (CNR), Italy
Tomohiro Hashizume,
University of Hamburg, Germany

*CORRESPONDENCE
Simon B. Jäger,
sjaeger2@uni-bonn.de

RECEIVED 27 November 2024
ACCEPTED 08 May 2025
PUBLISHED 19 June 2025

CITATION
Jäger SB (2025) Cooling strongly self-organized particles using adiabatic demagnetization.
Front. Quantum Sci. Technol. 4:1535581.
doi: 10.3389/frqst.2025.1535581

Cooling strongly self-organized particles using adiabatic demagnetization

Simon B. Jäger *

Physikalisches Institut, University of Bonn, Bonn, Germany

This study examines the dynamics of polarizable particles, coupled to a lossy cavity mode, that are transversally driven by a laser. The analysis is performed in a regime where the cavity linewidth exceeds the recoil frequency by several orders of magnitude. Using a two-stage cooling protocol, we show that the particles' kinetic energy can be reduced to the recoil energy. This cooling protocol relies in its first stage on a high laser power such that the particles cool into a strongly self-organized pattern. This can be seen as a strongly magnetized state. In a second stage, we adiabatically ramp down the laser intensity such that the particles' kinetic energy is transferred to their potential energy and the particles are "demagnetized". In this second stage, we optimize the ramping speed, which needs to be fast enough to avoid unwanted heating and slow enough such that the dynamics remains approximately adiabatic.

KEYWORDS

adiabatic demagnetization, cavity QED, semiclassical dynamic simulation, self-organization, stochastic differential equation, cavity cooling

1 Introduction

The realization of quantum technologies (Ladd et al., 2010; Acín et al., 2018; Barzanjeh et al., 2022) based on polarizable particles such as atoms, ions, molecules, and nanoparticles relies on the precise control of their motional degrees of freedom. One important step for achieving full control of these particles is to reduce their residual motion. A key technique to achieve this is laser cooling (Wineland and Itano, 1979; Chu, 1998; Wieman et al., 1999; Cohen-Tannoudji, 1998; Phillips, 1998; Stenholm, 1986; Metcalf and Van der Straten, 1999), which can be used to achieve temperatures that leave particles close to their zero-point motion. The basic principle behind laser cooling is the enhanced absorption rate of laser photons that lower the particle's momentum. Subsequently, incoherent scattering of a photon from the particle into free space results in lower kinetic energy of the particle. Despite the great success of laser cooling, one major problem is that it typically relies on closed transitions and the atomic species at hand. This hinders the universal application of conventional laser cooling techniques to more complex systems such as molecules or nanoparticles.

A good candidate for overcoming this problem is cavity cooling, where a particles' motion is cooled by coherent scattering of laser photons (Horak et al., 1997; Vuletić and Chu, 2000; Domokos et al., 2001; Domokos and Ritsch, 2002; Black et al., 2003; Maunz et al., 2004; Morigi et al., 2007; Schleier-Smith et al., 2011; Wolke et al., 2012; Hosseini et al., 2017). Here, the particles' kinetic energy is carried away by the scattered cavity photons while the internal state of the particles' remain almost unaltered. The simplest form of cavity cooling requires driving with a laser frequency that is red-detuned with respect to the cavity

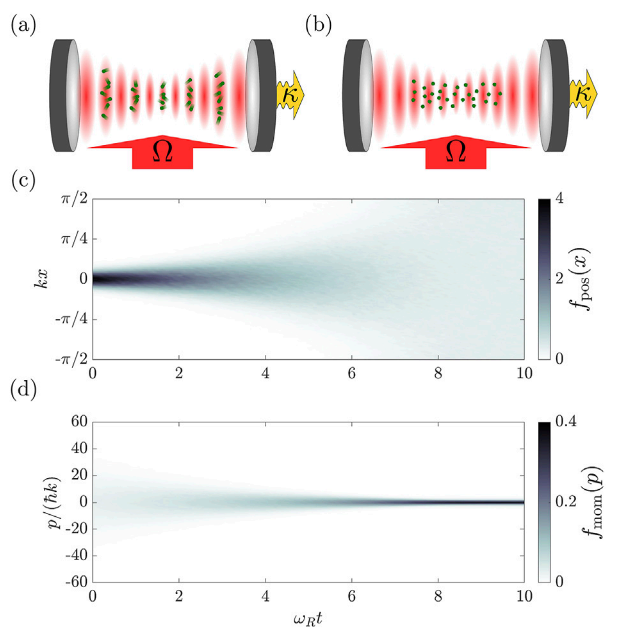

FIGURE 1
Particles are transversally driven by a laser with Rabi frequency Ω while dissipation of cavity photons is modeled by κ. **(a)** State of the particles after the first stage: the kinetic energy is determined by the cavity linewidth and the particles form a strongly self-organized pattern. **(b)** State of the particles after the second stage: kinetic energy is smaller while they are distributed homogeneously in space. The position distribution $f_{pos}(x)$ **(c)** as function of x in units of k^{-1} and the momentum distribution $f_{mom}(p)$ **(d)** as a function of p in units of $\hbar k$ and as functions of time t in units of ω_R^{-1} in the second stage. Magnetization, determined by the localization of the particles around $kx \approx 0$, decreases adiabatically while kinetic energy also decreases.

resonance. That way the cavity promotes the emission of blue-shifted photons which leaves the atoms in average at lower energy. In such a setup the minimum temperature is typically bounded by the linewidth of the cavity (Domokos et al., 2001). Cavity cooling of single atoms (Maunz et al., 2004) and collective cooling (Black et al., 2003; Hosseini et al., 2017) have been realized in experimental labs. Since cavity cooling does not rely on incoherent scattering from a specific internal state, it is has been proposed for cooling molecules (Morigi et al., 2007) and experimentally realized for cooling nanoparticles (Asenbaum et al., 2013; Delić et al., 2019). Although sub-recoil cooling has been achieved experimentally (Wolke et al., 2012) in an optical cavity with very narrow linewidth, the limit set by the cavity linewidth usually lies well above the recoil limit.

This paper investigates a situation where the cavity linewidth is orders of magnitude larger than the recoil frequency, which is, for instance, the case for the experiment described in Hosseini et al. (2017) but also in several other experiments. We demonstrate that it is theoretically possible to achieve temperatures that are of the order of a single recoil by using a combination of cavity cooling and adiabatic control of optomechanical forces. The key ingredient is that the scattered photons, besides cooling, also mediate collective interactions which allow the particles to self-organize (Domokos and Ritsch, 2002; Asbóth et al., 2005). Self-organization occurs if the driving-laser power exceeds a threshold determined by the cavity parameters and the temperature of the particles. Here, the particles spontaneously form a pattern with a spacing that is determined by the wavelength of the light and allows for the constructive interference of scattered photons. Atomic self-organization has been observed with ultra-cold bosons (Baumann et al., 2010), thermal atoms (Arnold et al., 2012), and ultra-cold fermions (Wu et al., 2023; Helson et al., 2023). The formation of a self-organized pattern can be described as a ferromagnetic phase of a long-range interacting system where the collectively scattered light field can be understood as a parameter that measures the magnetization of the atomic ensemble (Schütz et al., 2015).

This study aims to present a protocol which can lower the kinetic energy of polarizable particles close to the recoil limit, even if the cavity linewidth is orders of magnitude wider. It thus proposes a two-stage cooling protocol that uses both cavity cooling and self-organization to bring the particles to a final kinetic energy that is of the order of the recoil energy. The first stage uses collective cavity cooling of many particles with high laser power. The final temperature of the particles is here mostly determined by the cavity linewidth while the particles form a strongly self-organized (magnetized) pattern (Figure 1a). For these parameters, while the atoms possess a rather high kinetic energy, they are tightly confined in space in a pattern which supports constructive interference of scattered laser photons. In the second stage, laser power is slowly decreased such that the magnetization of the particles is adiabatically decreased (Figure 1c). Like the magnetocaloric effect and the principle of adiabatic demagnetization (Tishin and Spichkin, 2003), this results in a decrease of the magnetization of the particles and simultaneously lowers their kinetic energy (Figure 1d). In contrast, however, we do not ramp an external magnetic field but the laser driving amplitude which effectively reduces the particle–particle interactions. This principle is also related to so-called release–retrap or adiabatic trap relaxation protocols which are common in optical lattices and are used to achieve low temperatures and high phase-space densities (DePue et al., 1999; Hu et al., 2017). In such protocols, the particles are cooled in tightly confined trapping potentials while a subsequent adiabatic trap relaxation lowers kinetic energy even further. In contrast, however, the demagnetization presented here is of a collective nature and comes from strong cavity-mediated atom–atom interactions instead of deep laser trapping. This is important, since it allows us to perform the demagnetization fast enough such that cavity shot noise does not significantly heat the system while decreasing the driving-laser power. At the end of this ramp, particles reach a final temperature that can be orders of magnitude lower than that of conventional cavity cooling while the particles reach a spatially homogeneous state (Figure 1b).

This paper is structured as follows. Section 2 introduces the semiclassical equations that are used to simulate the system. Furthermore, we show analytical predictions for final kinetic energy following an adiabatic ramp. In Section 3, we analyze the effects of dissipation and show the actual proposed cooling protocol. Conclusions are drawn in Section 4, and Supplementary Appendix A provides details of the calculations in Section 2.

2 Physical setup

We consider a setup of N transversally driven polarizable particles with mass m inside a single-mode cavity. The particles are driven far off-resonant with detuning $\Delta_a = \omega_L - \omega_a$ between laser frequency ω_L and transition frequency ω_a such that spontaneous emission and the population of the excited state can be neglected. The laser light is thus coherently scattered with rate $S = g\Omega/\Delta_a$ by the particles into the cavity. Here, Ω is the Rabi frequency of the driving-laser field and g is the vacuum Rabi frequency of the cavity. We assume that the coupling between the particles and the cavity is proportional to the mode function $\cos(kx)$ where k denotes the wave number of the cavity mode. The laser frequency is red-detuned to the frequency ω_c of the single resonator mode with detuning $\Delta_c = \omega_L - \omega_c < 0$. Furthermore, the cavity mode loses photons at rate κ. In what follows, we discard effects of the dynamical stark shift $U = g^2/\Delta_a$. This is possible if Δ_c and κ are much larger than NU.

2.1 Semiclassical description

We now present a semiclassical description of the particles' center of mass motion and the cavity field. The coupled equations for the motion of the particles with position x_j and momentum p_j, and the real and imaginary part of the cavity field $\mathcal{E}_r$ and $\mathcal{E}_i$ evolve according to the following stochastic differential equations (Domokos et al., 2001)

$$dx_j = \frac{p_j}{m}dt, \tag{1a}$$

$$dp_j = 2\hbar kS\mathcal{E}_r \sin\left(kx_j\right)dt, \tag{1b}$$

$$d\mathcal{E}_r = (-\Delta_c\mathcal{E}_i - \kappa\mathcal{E}_r)dt + d\xi_r, \tag{1c}$$

$$d\mathcal{E}_i = (\Delta_c\mathcal{E}_r - \kappa\mathcal{E}_i - NS\Theta)dt + d\xi_i, \tag{1d}$$

and $j = 1, 2, \ldots, N$. The noise terms $d\xi_i, d\xi_r$ have vanishing first moments, $\langle d\xi_i\rangle = 0 = \langle d\xi_r\rangle$, while the second moments fulfill $\langle d\xi_i d\xi_i\rangle = \kappa dt/2$, $\langle d\xi_r d\xi_r\rangle = \kappa dt/2$, and $\langle d\xi_r d\xi_i\rangle = 0$. Furthermore, the order parameter or magnetization Θ is defined by

$$\Theta = \frac{1}{N}\sum_{j=1}^{N}\cos\left(kx_j\right). \tag{2}$$

Equations 1a, b, c, and d describe the driven-dissipative dynamics of the particles that couple to a dissipative cavity mode.

To better understand the forces that are mediated by the cavity, it is useful to eliminate the cavity degrees of freedom from the dynamics. Here, we work in the limit where $\kappa, |\Delta_c| \gg k\Delta p/m$ and $\kappa^2 \gg \omega_R\sqrt{NS}$, with $\omega_R = \hbar k^2/(2m)$ the recoil frequency. This implies that the cavity degrees evolve much faster and can be adiabatically eliminated (Schütz et al., 2013). Here, $k\Delta p/m$ is the Doppler-width and Δp is the single-particle momentum width. Working in this regime allows us to simplify Equations 1a, b, c, and d by calculating the adiabatic stationary state of the cavity field. This is done by formally integrating the differential equations for $\mathcal{E}_r$ and $\mathcal{E}_i$. The adiabatic solution is given by

$$\mathcal{E}_r = \frac{\Delta_c NS\Theta}{\Delta_c^2 + \kappa^2}, \tag{3}$$

$$\mathcal{E}_i = \frac{-\kappa NS\Theta}{\Delta_c^2 + \kappa^2}. \tag{4}$$

Using this result in Equations 1a, b, c, and d results in

$$dx_j = \frac{p_j}{m}dt, \tag{5a}$$

$$dp_j = -2kV\sin\left(kx_j\right)\Theta dt, \tag{5b}$$

with

$$V = -\hbar\Delta_c\frac{NS^2}{\Delta_c^2 + \kappa^2}.$$

We emphasize that V is positive since we assumed $\Delta_c < 0$, which allows for self-organization and cavity cooling (Asbóth et al., 2005). The dynamics given by Equation 5a, b can be rewritten using an effective Hamiltonian

$$H_{\text{eff}} = \sum_j \frac{p_j^2}{2m} - NV\Theta^2,$$

with $dx_j/dt = \partial H_{\text{eff}}/\partial p_j, dp_j/dt = -\partial H_{\text{eff}}/\partial x_j$. The term $\propto V$ is a long-range interaction potential which tries to maximize the value of Θ. The latter is the order parameter or magnetization and is used to distinguish between the self-organized and the spatially homogeneous phase. In this context, the values of $\cos(kx_j)$ can be seen as a continuous magnetization for each atom which takes values between -1 and $+1$. In the spatially homogeneous or paramagnetic phase, $\cos(kx_j)$ takes random values between -1 and $+1$ such that $\Theta \approx 0$. In the self-organized or ferromagnetic phase, the particles form a pattern with a periodicity that is determined by the wavelength $\lambda = 2\pi/k$ such that $|\Theta| > 0$, meaning that the individual spins fulfil either all $\cos(kx_j) \approx 1$ or all $\cos(kx_j) \approx -1$. In an experiment, the magnetization can be detected from the cavity output. This can be seen by finding the stationary state of Equations 1c, d that can be used to calculate the intra-cavity photon number

$$I = \langle\mathcal{E}_r^2 + \mathcal{E}_i^2\rangle \approx \frac{N^2S^2}{\Delta_c^2 + \kappa^2}\langle\Theta^2\rangle, \tag{6}$$

where we used Equations 3, 4 and the average runs over different initializations and trajectories.

After adiabatic elimination of the cavity degrees of freedom, we derived a dynamical description from a classical Hamiltonian. This implies that Equations 5a, b conserve the mean energy $\langle H_{\text{eff}}\rangle$ for a time-independent interaction strength V. The description by means of Hamiltonian dynamics is, however, only true on a timescale where dissipative effects can be discarded (Schütz et al., 2015; Schütz et al., 2013; Schütz and Morigi, 2014; Jäger et al., 2016; Schütz et al., 2016).

In the following, we are interested in changing V very slowly such that the particles evolve mainly adiabatically but do so sufficiently fast such that dissipative effects are negligible.

2.2 Adiabatic ramp of the interaction strength

We assume that the distribution function of the particles is given by a thermal state which can be seen as the stationary state of the system reached after sufficiently long times. This state is given by

$$f_t(\mathbf{x},\mathbf{p}) = Z^{-1}(\beta_t)e^{-\beta_t H_{\text{eff}}}$$

with single-particle kinetic energy

$$E^{\text{kin}}(t) = \frac{\langle p^2\rangle(t)}{2m} = \frac{1}{2\beta_t}, \tag{7}$$

and partition function $Z(\beta_t) = \int d\mathbf{x}\int d\mathbf{p}e^{-\beta_t H_{\text{eff}}}$. Note that f_t and β_t are explicitly time-dependent. The expectation value is here defined by $\langle h(\mathbf{x},\mathbf{p})\rangle(t) = \int d\mathbf{x}\int d\mathbf{p}h(\mathbf{x},\mathbf{p})f_t(\mathbf{x},\mathbf{p})$ with integrals $\int d\mathbf{x} = \int_0^\lambda dx_1\ldots\int_0^\lambda dx_N$ and $\int d\mathbf{p} = \int_{-\infty}^{\infty} dp_1\ldots\int_{-\infty}^{\infty} dp_N$ and for an arbitrary function $h(\mathbf{x},\mathbf{p})$ of the atomic positions and momenta.

We assume a time dependent V and, in particular, that the temporal change of V is sufficiently slow such that the particles remain in a thermal state. With this assumption, a dynamical equation for the kinetic energy can be derived in the following.

Using Equations 5a, b and Equation 7, we obtain the dynamical evolution of the single-particle kinetic energy

$$\frac{dE^{\text{kin}}}{dt} = V\frac{d\langle\Theta^2\rangle}{dt}. \tag{8}$$

Furthermore, we may write

$$\langle\Theta^2\rangle = \left.\frac{dF}{dy}\right|_{y=\frac{NV}{2E^{\text{kin}}}}$$

with

$$F(y) = \ln\left(\int d\mathbf{x}e^{y\Theta^2}\right).$$

Then, using $V = 2E^{\text{kin}}y/N$, we can rewrite Equation 8 as

$$N\frac{dE^{\text{kin}}}{dy} = 2E^{\text{kin}}y\frac{d^2F(y)}{dy^2},$$

and the integration of this equation leads to

$$\int_{E_0^{\text{kin}}}^{E_1^{\text{kin}}}\frac{dE^{\text{kin}}}{E^{\text{kin}}} = \int_{y_0}^{y_1} dy\frac{2y}{N}\frac{d^2F}{dy^2},$$

where $y_n = NV_n/(2E_n^{\text{kin}})$ with $n = 0, 1$. The latter can be solved using integration by parts to obtain

$$\ln\left(\frac{E_1^{\text{kin}}}{E_0^{\text{kin}}}\right) = \frac{2}{N}\left[y\frac{dF(y)}{dy} - F(y)\right]_{y_0}^{y_1},$$

using the notation $[f(y)]_{y_0}^{y_1} = f(y_1) - f(y_0)$. Defining $\alpha_n = y_n/N = V_n/(2E_n^{\text{kin}})$ and performing the limit $N\to\infty$ with $\alpha_n = \text{const}$ we obtain the result

$$\frac{E_1^{\text{kin}}}{E_0^{\text{kin}}} = \left[\frac{I_0(2\alpha_0\theta(\alpha_0))e^{-2\alpha_0\theta^2(\alpha_0)}}{I_0(2\alpha_1\theta(\alpha_1))e^{-2\alpha_1\theta^2(\alpha_1)}}\right]^2, \tag{9}$$

where I_n is the nth modified Bessel function and $\theta(\alpha)$ describes the stable solution of the equation

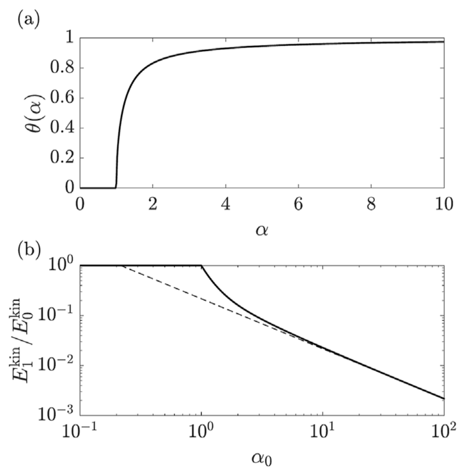

FIGURE 2
(a) The stable solution $\theta(\alpha)$ of Equation 10 as function of α. **(b)** Quotient of final E_1^{kin} and initial kinetic energy E_0^{kin} depending on α_0 given by Equation 11. The dashed line is the asymptotic result given by Equation 12.

$$\theta = \frac{I_1(2\alpha\theta)}{I_0(2\alpha\theta)}. \tag{10}$$

See Supplementary Appendix A for a detailed derivation. The value for θ calculated from Equation 10 is the mean magnetization of the particles for the given value of α. Thus, Equation 9 connects the magnetization before and after the ramp with the kinetic energy before and after the ramp. We now discuss how this result can be used to lower the kinetic energy of the particles.

In Figure 2a we plotted $\theta(\alpha)$ as a function of α. It can be seen that $\theta(\alpha)$ is 0 for $\alpha < 1$ (paramagnetic phase) and increases for $\alpha > 1$ (ferromagnetic phase) while it tends to 1 in $\alpha\to\infty$. Note that only the positive solution $\theta > 0$ has been shown, but there is also the solution $-\theta$. This transition from spatially homogeneous (paramagnetic) to self-organized (ferromagnetic) has been described as a "phase transition."

In the spatially homogeneous phase, for $\alpha_1, \alpha_0 \leq 1$, the quotient of the kinetic energies in Equation 9 is always 1. This implies that any adiabatic change within the spatially homogeneous region will, to good approximation, not affect the kinetic energy.

However, when we assume that the coupling strength is initialized such that the particles are in the self-organized phase and ramped to a value where the particles are distributed spatially homogeneously—that is, $\alpha_0 > 1$ and $\alpha_1 \leq 1$—we obtain

$$\frac{E_1^{\text{kin}}}{E_0^{\text{kin}}} = \left[I_0(2\alpha_0\theta(\alpha_0))e^{-2\alpha_0\theta^2(\alpha_0)}\right]^2. \tag{11}$$

This result of the right-hand side of Equation 11 in Figure 2b is shown as black solid line. It is a monotonous decreasing function with α_0. Therefore, we conclude that a potentially very low kinetic energy can be reached by starting the ramp from a high coupling strength V_0. In this regime, for $\alpha_0 \gg 1$, we obtain the asymptotic result

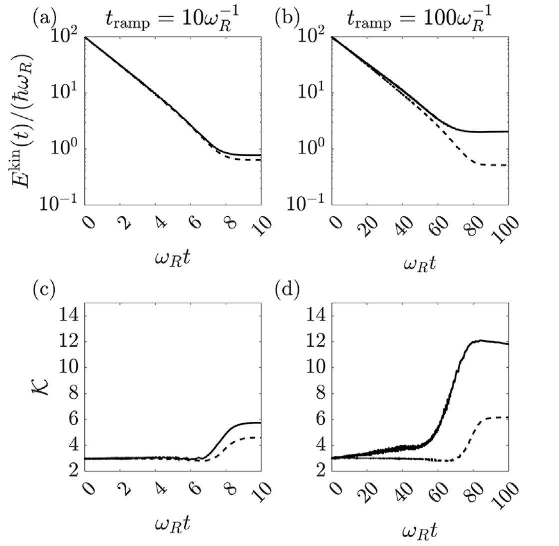

FIGURE 3
The kinetic energies E^{kin} in units of $\hbar\omega_R$ **(a,b)** and the kurtosis $\mathcal{K}$ (Equation 14) **(c,d)** as function of time t in units of ω_R^{-1} following a ramp according to Equation 13 with $t_{\mathrm{ramp}} = 10\omega_R^{-1}$ and $t_{\mathrm{ramp}} = 100\omega_R^{-1}$, respectively. We have chosen $V_0 = 10^4\hbar\omega_R$, $\Delta_c = -\kappa$, $\kappa = 400\omega_R$, $N = 100$, and $NS_0^2 = 50\kappa^2$ and averaged over 200 trajectories. The system is initialized in a strongly self-organized thermal state with $E^{\mathrm{kin}}(0) = 100\hbar\omega_R$.

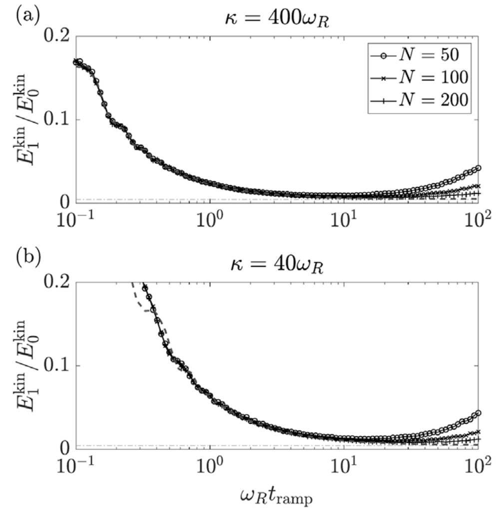

FIGURE 4
Final kinetic energy $E_1^{\mathrm{kin}} = E^{\mathrm{kin}}(t_{\mathrm{ramp}})$ in units of $E_0^{\mathrm{kin}} = \hbar\kappa/4$ for different ramping times t_{ramp} in units of ω_R^{-1} and for **(a)** $\kappa = 400\omega_R$ and **(b)** $\kappa = 40\omega_R$. The simulations have been performed for different particle numbers (see inset of (a)) using Equations 1a, b, c, d. The dashed gray lines correspond to simulations of Equations 5a and b with $N = 200$ particles. The horizontal dashed–dotted gray lines are the predictions of Equation 12. All results are obtained for simulations with parameters $\Delta_c = -\kappa$, $\alpha_0 = V_0/(2E_1^{\mathrm{kin}}) = 50$ and using $20000/N$ trajectories.

$$\frac{E_1^{\mathrm{kin}}}{E_0^{\mathrm{kin}}} = \frac{e}{4\pi\alpha_0}, \tag{12}$$

where e is the Euler number. This shows that the ratio of the kinetic energies is proportional to $1/\alpha_0$ and is plotted as a dashed gray line in Figure 2b.

We now discuss how this principle might be applicable to the driven-dissipative dynamics of particles in a cavity.

3 Cooling protocol

In order to apply the results of the previous section, we must first analyze the dissipative effects in the particles' dynamics. This is done by comparing the results of Equations 5a, b that discard any dissipative effects with the dynamics, including dissipation, in Equations 1a, b, c, d.

3.1 Effects of dissipation

We first initialize the particles in a strongly self-organized thermal state with kinetic energy E^{kin} Then, we ramp V exponentially as

$$V(t) = V_0 \cdot 10^{-5\frac{t}{t_{\mathrm{ramp}}}}, \tag{13}$$

for different ramping times t_{ramp}. While the choice of an exponential ramp is a technical detail, it allows for a rather fast change of the interaction strength for large values of $V \approx V_0$ and slow changes for $V \gtrsim 0$. This seems a good compromise between being fast and remaining approximately adiabatic. We study the dynamics of the full system, including the cavity degrees of freedom (Equations 1a, b, c, d) and the dynamics where the cavity degrees of freedom are eliminated (Equations 5a, b). Figures 3a, b show the dynamics of the kinetic energy following the ramp for a ramping time of $t_{\mathrm{ramp}} = 10\omega_R^{-1}$ and $t_{\mathrm{ramp}} = 100\omega_R^{-1}$, respectively. To put these values into actual numbers, we provide an explicit example and use the value $\omega_R = 2\pi \times 2\,\mathrm{kHz}$ from Hosseini et al. (2017) for ^{133}Cs, which results in ramping times $t_{\mathrm{ramp}} \approx 1\,\mathrm{ms}$ and $t_{\mathrm{ramp}} \approx 10\,\mathrm{ms}$, respectively. The dashed line shows the result using the conservative dynamics (Equation 5a, b), while the solid line represents the full dissipative dynamics (Equation 1a, b, c, d). Both curves for both ramping times show decreased kinetic energy. There is good agreement of both dynamics on short timescales while we observe discrepancies for the longer ramping time. Therefore, we expect that for sufficiently short times, dissipative effects are still negligible while they affect the dynamics on longer timescales. This relies on a timescale separation of dissipative and conservative forces that relies on (i) the number of particles and (ii) the typical timescale separation of motion and cavity relaxation—that is, $k\Delta p/m \ll \kappa$. This was studied by Jäger et al., (2016) and Schütz et al., (2016) and observed in Wu et al. (2023). In conclusion, this preliminary analysis demonstrates that there must be an optimal ramping time for which the lowest possible temperature can be achieved.

While our original assumption was that the ramp is close to adiabatic, we expect this assumption to fail, especially because the system parameters are ramped across a phase transition. An observable to test this is the kurtosis

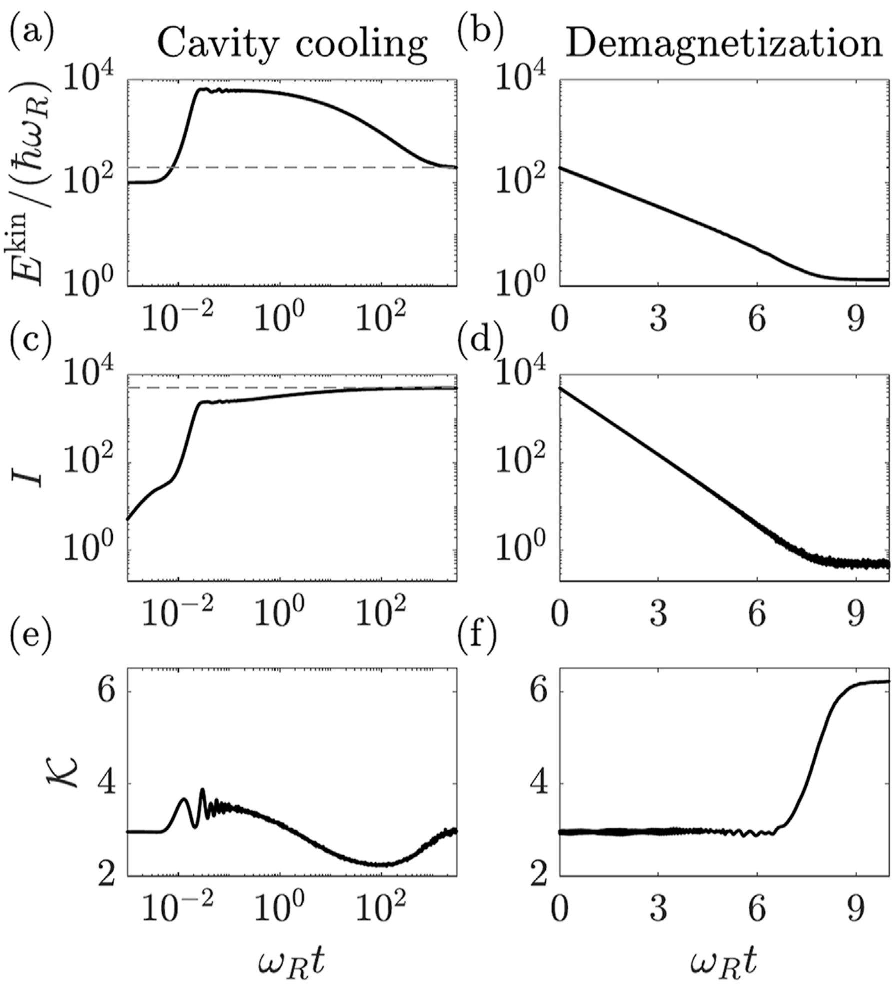

FIGURE 5
Dynamics of the kinetic energies E^{kin} in units of $\hbar\omega_R$ **(a,b)**, cavity field determined by Equation 6 **(c,d)**, and kurtosis $\mathcal{K}$ (Equation 14) **(e,f)** as a function of time t in units of ω_R^{-1}. The plots in **(a,c,e)** are obtained after a quench from $V \approx 0$ to $V = V_{\mathrm{fer}}^{\mathrm{opt}}$ (Equation 18), where the particles are initialized in a spatially homogeneous state with Gaussian momentum distribution and initial kinetic energy $E^{\mathrm{kin}}(0) = \hbar\kappa/4$. After a relaxation time $t_f = 3 \times 10^3\omega_R^{-1}$, we perform a ramp according to Equation 13 resulting in the dynamics visible in **(b,d,f)**. The ramping time is $t_{\mathrm{ramp}} = 10\omega_R^{-1}$, and all simulations have been performed with $\Delta_c = -\kappa$, $\kappa = 400\omega_R$, $N = 100$, and averaging over 200 trajectories.

$$\mathcal{K}(t) = \frac{\langle p^4\rangle(t)}{\left[\langle p^2\rangle(t)\right]^2}. \tag{14}$$

The kurtosis is $\mathcal{K} = 3$ for a Gaussian state and deviates from 3 for non-Gaussian states. Figures 3c, d show the kurtosis with the same labeling for the two different ramping times. In Figure 3c, we observe that the kurtosis remains close to 3 for times $t \lesssim 7\omega_R^{-1}$, while it deviates for longer times as soon as the value of V crosses the phase transition line. In Figure 3d we observe the same for the simulations of the conservative dynamics (Equations 5a, b) and times $t \lesssim 70\omega_R^{-1}$, while the simulation of the full dissipative dynamics (Equations 1a, b, c, d) shows values of $\mathcal{K} \neq 3$ on much shorter timescales. This finding supports our claim that the dynamics do not remain adiabatic across the phase transition. In addition, the discrepancies between the conservative and dissipative dynamics predict a dissipation-assisted creation of non-Gaussian states that is closely related to the dissipation-assisted stabilization of non-Gaussian states predicted in Schütz et al. (2016).

We now analyze the dependence of the minimum achievable temperature on the ramping time t_{ramp}. Figure 4 compares the values of the final kinetic energies $E_1^{\mathrm{kin}} = E^{\mathrm{kin}}(t_{\mathrm{ramp}})$ for different ramping times t_{ramp}, different particle numbers, and different ratios of κ/ω_R. The black line with symbols are calculated using simulations of Equations 1a, b, c, d with $N = 50$ (circles), $N = 100$ (crosses), and $N = 200$ (pluses), where we show $\kappa = 400\omega_R$ in Figure 4a and $\kappa = 40\omega_R$ in Figure 4b. These are realistic values, and the lower value of $\kappa = 40\omega_R$ is close to that realized in Hosseini et al. (2017). For both simulations, the system has been initialized with a pumping strength of $\alpha_0 = V_0/(2E_0^{\mathrm{kin}}) = 50$ and $E_1^{\mathrm{kin}} = \hbar\kappa/4$. The results of the simulations predict a local minimum of the kinetic energy in the range $\omega_R t_{\mathrm{ramp}} = 10 - 100$, thus showing that there is an optimal ramping time. In general, this optimal ramping time is shorter for smaller particle numbers. In addition, the minimum achievable kinetic energy is larger for smaller particle numbers. This should be due to the timescale separation between the conservative and dissipative forces that becomes larger for increasing particle numbers.

We also find that the result of the kinetic energy for $\kappa = 40\omega_R$ (b) appears to be slightly displaced to larger ramping times with respect to the simulations for $\kappa = 400\omega_R$ (a). We expect that this is due to a violation of the adiabaticity criteria, $\kappa t_{\mathrm{ramp}} \gg 1$ and $k\Delta p t_{\mathrm{ramp}}/m \gg 1$, that are not fulfilled for smaller values of $k\Delta p/m$ and κ and short ramping times in Figure 4b. For completeness, we have also included a simulation of Equations 5a and b that does not include dissipation and noise. The results are visible as gray dashed lines in Figure 4. Those curves are monotonically decreasing, thus showing that noise and dissipation are the origins for the local minima in the kinetic energy in the full simulations. The theoretical minimum of the achievable kinetic energy is shown as a gray dashed–dotted line. It is calculated using Equation 12 and $\alpha_0 = 50$, resulting in $E_1^{\mathrm{kin}}/E_0^{\mathrm{kin}} \approx 0.04$. We observe that the simulation without dissipation and noise (gray dashed line) converges to this theoretical minimum in the limit $\omega_R t_{\mathrm{ramp}} \to \infty$.

3.2 Cooling protocol

We now use this gained insight to minimize the kinetic energy of particles that are initially in a spatially homogeneous configuration. We thus assume that the initial state is a thermal state with temperature $k_B T_{\mathrm{in}} = \hbar\kappa/2$ that can be reached by cavity cooling for $\Delta_c = -\kappa$. The actual choice of this state is rather arbitrary but should be sufficiently cold such that the ensemble can be cavity (laser) cooled.

In a first stage, we perform a quench in the driving-laser intensity determined by S such that V has a value V_{fer} for the system to reach a state well inside the self-organized phase. Over a very long time, the system again reaches a stationary state which is thermal. To be consistent, for large laser intensities, we need to take corrections of the final temperature into account which come from the laser driving power. This final kinetic energy is given in the well-organized regime (Niedenzu et al., 2011; Grießer et al., 2012) by

$$E_{\mathrm{fer}}^{\mathrm{kin}} = \frac{k_B T_{\mathrm{fer}}}{2} = \frac{\hbar\left(\Delta_c^2 + \kappa^2 + 4\omega_0^2\right)}{-8\Delta_c}, \tag{15}$$

where $\omega_0^2 = 4\omega_R \frac{V_{\mathrm{fer}}}{\hbar}$ is the effective trapping frequency.

In a second stage, we consider a ramp from V_{fer} back to a value close to 0 such that both magnetization and kinetic energy are adiabatically reduced. If we assume that the system remains adiabatic in a thermal state, the optimum final kinetic energy can be approximated using Equation 12 by

$$E_{\mathrm{par}}^{\mathrm{kin}} = \frac{e}{2\pi}\frac{\left(E_{\mathrm{fer}}^{\mathrm{kin}}\right)^2}{V_{\mathrm{fer}}}. \tag{16}$$

By minimizing Equation 16 with respect to V_{fer}, we find

$$E_{\mathrm{min}}^{\mathrm{kin}} = \frac{e}{2\pi}\hbar\omega_R\frac{\Delta_c^2 + \kappa^2}{\Delta_c^2} \tag{17}$$

at an optimum value of

$$V_{\mathrm{fer}}^{\mathrm{opt}} = \frac{\hbar\left(\Delta_c^2 + \kappa^2\right)}{16\omega_R}. \tag{18}$$

This minimum kinetic energy is of the order of the recoil energy $\hbar\omega_R$.

We now consider simulations that test this prediction. Following the procedure of the first stage, Figure 5a shows the dynamics of the kinetic energy after a quench from $V \approx 0$ to $V = V_{\mathrm{fer}}^{\mathrm{opt}}$ (Equation 18). Initially, a rapid increase is observed in the magnetization determined by $\langle\Theta^2\rangle$. This can be seen in Figure 5c, which plots the cavity field determined by Equation 6. Since energy is conserved on short timescales, the kinetic energy is also exponentially increasing, reaching a maximum of $E^{\mathrm{kin}} \approx 6.5 \times 10^3 \ \hbar\omega_R$. On longer timescales, dissipation guides the system toward a thermal state with a temperature given by Equation 15 (horizontal gray dashed line in Figure 5a) with corresponding magnetization (horizontal gray dashed line in Figure 5c). The steady-state magnetization has been calculated using $\langle\Theta^2\rangle \approx \theta^2$ where θ is the solution of Equation 10. Figure 5e plots the kurtosis (Equation 14) that starts and ends at a value close to $\mathcal{K} \approx 3$, suggesting that both the final and initial state are thermal.

Following the second stage, we ramp the coupling strength according to Equation 13 with a ramping time of $t_{\mathrm{ramp}} = 10\omega_R^{-1}$ that we have found to be close to optimal for the choice of parameters in the previous subsection. Figure 5b shows the decrease of the kinetic energy that eventually reaches a value that is of the order of the recoil energy. We observe a final kinetic energy of $E_{\mathrm{final}}^{\mathrm{kin}} = 1.3\hbar\omega_R$, whereby Equation 17 predicts a similar value of $E_{\mathrm{min}}^{\mathrm{kin}} \approx 0.9\hbar\omega_R$. During this process, the field intensity and mean magnetization of the system are decreased (Figure 5d), reminiscent of adiabatic demagnetization. We emphasize that the adiabatic process is much faster than cavity cooling in the first stage. This is visible by comparing the time axes in Figures 5a and b. This difference in the timescales comes from the fact that the adiabatic process is collective. The kurtosis, visible in Figure 5f, remains 3 during the ramp until the phase transition line is crossed and the process is no longer adiabatic.

4 Conclusion

In this paper, we have studied the possibility of cooling transversally driven particles inside an optical cavity using a combination of cavity cooling and a protocol reminiscent of adiabatic demagnetization. To analyze the effect of dissipation, we have performed simulations of dissipative and conservative dynamical models for this physical setup. We have shown that the particles can reach kinetic energies comparable to the recoil limit for the parameter choice below the typical limit of cavity cooling. To achieve this final kinetic energy, we have tuned the laser power from a value well above the self-organization threshold to below it. The duration of this ramp is chosen sufficiently long such that it seems to be quasi-adiabatic for the coherent dynamics but sufficiently rapid such that dissipation has only a minor effect on the final kinetic energy.

While the results presented here rely on adiabatically changing the coupling or interaction strength that results in a change of the internal magnetization, we expect that similar physics can be achieved by changing an additional external field that simulates an effective magnetic field. This can, for instance, be accomplished by modulating a laser that directly drives the cavity beside the transversal laser field (Niedenzu et al., 2013).

It is important to emphasize that the cooling stage is crucial to achieving the final kinetic energy as it reduces entropy. However, the precise cooling protocol is rather arbitrary. In particular, the choice of cavity cooling, visible in Figure 5, can be replaced by other schemes, such as a ramp of the interaction strength instead of a quench, or even by other laser cooling mechanisms. Importantly, the sole outcome of this first stage is the preparation of a sufficiently cold and highly self-organized (magnetized) particle ensemble.

Regarding the ultimate limits of this cooling protocol, this analysis is performed with semiclassical equations. This means our approach is only valid for kinetic energies that are above the recoil limit. In addition, we have not included the quantum statistics of the particles, which becomes relevant for low temperatures. Including the latter would be an interesting extension of our work since one might expect different distributions for bosons (Baumann et al., 2010) and fermions (Helson et al., 2023; Zhang et al., 2021). In future research, it might also be interesting to use multi-mode cavities that provide more possibilities to tune the interactions and dissipation (Torggler and Ritsch, 2014; Keller et al., 2017; Keller et al., 2018). The study of such systems is not only interesting for advances in laser and cavity cooling but also as a simulator for classical and quantum thermodynamics (Vinjanampathy and Anders, 2016; Niedenzu et al., 2018). In conclusion, the engineering of interactions and dissipation for particles in optical cavities is a versatile tool for quantum technologies and studying new physics.

Data availability statement

The raw data supporting the conclusions of this article will be made available by the author without undue reservation.

Author contributions

SJ: Writing – original draft and Writing – review and editing.

Funding

The author(s) declare that financial support was received for the research and/or publication of this article. We acknowledge support from the Deutsche Forschungsgemeinschaft (DFG, German Research Foundation) under project number 277625399—TRR 185 (B4) and under Germany's Excellence Strategy—Cluster of Excellence Matter and Light for Quantum Computing (ML4Q) EXC 2004/1—390534769.

Acknowledgments

SJ acknowledges stimulating discussions with Stefan Schütz, John Cooper, and Giovanna Morigi.

Conflict of interest

The author declares that the research was conducted in the absence of any commercial or financial relationships that could be construed as a potential conflict of interest.

Generative AI statement

The author(s) declare that no Generative AI was used in the creation of this manuscript.

Publisher's note

Supplementary material

The Supplementary Material for this article can be found online at: https://www.frontiersin.org/articles/10.3389/frqst.2025.1535581/full#supplementary-material

References

Acín, A., Bloch, I., Buhrman, H., Calarco, T., Eichler, C., Eisert, J., et al. (2018). The quantum technologies roadmap: a european community view. *New J. Phys.* 20, 080201. doi:10.1088/1367-2630/aad1ea

Arnold, K. J., Baden, M. P., and Barrett, M. D. (2012). Self-organization threshold scaling for thermal atoms coupled to a cavity. *Phys. Rev. Lett.* 109, 153002. doi:10.1103/physrevlett.109.153002

Asbóth, J. K., Domokos, P., Ritsch, H., and Vukics, A. (2005). Self-organization of atoms in a cavity field: threshold, bistability, and scaling laws. *Phys. Rev. A* 72, 053417. doi:10.1103/physreva.72.053417

Asenbaum, P., Kuhn, S., Nimmrichter, S., Sezer, U., and Arndt, M. (2013). Cavity cooling of free silicon nanoparticles in high vacuum. *Nat. Commun.* 4, 2743. doi:10.1038/ncomms3743

Barzanjeh, S., Xuereb, A., Gröblacher, S., Paternostro, M., Regal, C. A., and Weig, E. M. (2022). Optomechanics for quantum technologies. *Nat. Phys.* 18, 15–24. doi:10.1038/s41567-021-01402-0

Baumann, K., Guerlin, C., Brennecke, F., and Esslinger, T. (2010). Dicke quantum phase transition with a superfluid gas in an optical cavity. *Nature* 464, 1301–1306. doi:10.1038/nature09009

Black, A. T., Chan, H. W., and Vuletić, V. (2003). Observation of collective friction forces due to spatial self-organization of atoms: from Rayleigh to bragg scattering. *Phys. Rev. Lett.* 91, 203001. doi:10.1103/physrevlett.91.203001

Chu, S. (1998). Nobel lecture: the manipulation of neutral particles. *Rev. Mod. Phys.* 70, 685–706. doi:10.1103/revmodphys.70.685

Cohen-Tannoudji, C. N. (1998). Nobel lecture: manipulating atoms with photons. *Rev. Mod. Phys.* 70, 707–719. doi:10.1103/revmodphys.70.707

Delić, U., Reisenbauer, M., Grass, D., Kiesel, N., Vuletić, V., and Aspelmeyer, M. (2019). Cavity cooling of a levitated nanosphere by coherent scattering. *Phys. Rev. Lett.* 122, 123602. doi:10.1103/physrevlett.122.123602

DePue, M. T., McCormick, C., Winoto, S. L., Oliver, S., and Weiss, D. S. (1999). Unity occupation of sites in a 3d optical lattice. *Phys. Rev. Lett.* 82, 2262–2265. doi:10.1103/physrevlett.82.2262

Domokos, P., Horak, P., and Ritsch, H. (2001). Semiclassical theory of cavity-assisted atom cooling. *J. Phys. B* 34, 187–198. doi:10.1088/0953-4075/34/2/306

Domokos, P., and Ritsch, H. (2002). Collective cooling and self-organization of atoms in a cavity. *Phys. Rev. Lett.* 89, 253003. doi:10.1103/physrevlett.89.253003

Grießer, T., Niedenzu, W., and Ritsch, H. (2012). Cooperative self-organization and sympathetic cooling of a multispecies gas in a cavity. *New J. Phys.* 14, 053031. doi:10.1088/1367-2630/14/5/053031

Helson, V., Zwettler, T., Mivehvar, F., Colella, E., Roux, K., Konishi, H., et al. (2023). Density-wave ordering in a unitary fermi gas with photon-mediated interactions. *Nature* 618, 716–720. doi:10.1038/s41586-023-06018-3

Horak, P., Hechenblaikner, G., Gheri, K. M., Stecher, H., and Ritsch, H. (1997). Cavity-induced atom cooling in the strong coupling regime. *Phys. Rev. Lett.* 79, 4974–4977. doi:10.1103/physrevlett.79.4974

Hosseini, M., Duan, Y., Beck, K. M., Chen, Y.-T., and Vuletić, V. (2017). Cavity cooling of many atoms. *Phys. Rev. Lett.* 118, 183601. doi:10.1103/physrevlett.118.183601

Hu, J., Urvoy, A., Vendeiro, Z., Crépel, V., Chen, W., and Vuletić, V. (2017). Creation of a bose-condensed gas of ^{87}rb by laser cooling. *Science* 358, 1078–1080. doi:10.1126/science.aan5614

Jäger, S. B., Schütz, S., and Morigi, G. (2016). Mean-field theory of atomic self-organization in optical cavities. *Phys. Rev. A* 94, 023807. doi:10.1103/physreva.94.023807

Keller, T., Jäger, S. B., and Morigi, G. (2017). Phases of cold atoms interacting via photon-mediated long-range forces. *J. Stat. Mech.* 2017, 064002. doi:10.1088/1742-5468/aa71d7

Keller, T., Torggler, V., Jäger, S. B., Schütz, S., Ritsch, H., and Morigi, G. (2018). Quenches across the self-organization transition in multimode cavities. *New J. Phys.* 20, 025004. doi:10.1088/1367-2630/aaa161

Ladd, T. D., Jelezko, F., Laflamme, R., Nakamura, Y., Monroe, C., and O'Brien, J. L. (2010). Quantum computers. *Nature* 464, 45–53. doi:10.1038/nature08812

Maunz, P., Puppe, T., Schuster, I., Syassen, N., Pinkse, P. W. H., and Rempe, G. (2004). Cavity cooling of a single atom. *Nature* 428, 50–52. doi:10.1038/nature02387

Metcalf, H. J., and Van der Straten, P. (1999). *Laser cooling and trapping*. Springer Science & Business Media.

Morigi, G., Pinkse, P. W. H., Kowalewski, M., and de Vivie-Riedle, R. (2007). Cavity cooling of internal molecular motion. *Phys. Rev. Lett.* 99, 073001. doi:10.1103/physrevlett.99.073001

Niedenzu, W., Grießer, T., and Ritsch, H. (2011). Kinetic theory of cavity cooling and self-organisation of a cold gas. *Europhys. Lett.* 96, 43001. doi:10.1209/0295-5075/96/43001

Niedenzu, W., Mukherjee, V., Ghosh, A., Kofman, A. G., and Kurizki, G. (2018). Quantum engine efficiency bound beyond the second law of thermodynamics. *Nat. Commun.* 9, 165. doi:10.1038/s41467-017-01991-6

Niedenzu, W., Schütz, S., Habibian, H., Morigi, G., and Ritsch, H. (2013). Seeding patterns for self-organization of photons and atoms. *Phys. Rev. A* 88, 033830. doi:10.1103/physreva.88.033830

Phillips, W. D. (1998). Nobel lecture: laser cooling and trapping of neutral atoms. *Rev. Mod. Phys.* 70, 721–741. doi:10.1103/revmodphys.70.721

Schleier-Smith, M. H., Leroux, I. D., Zhang, H., Van Camp, M. A., and Vuletić, V. (2011). Optomechanical cavity cooling of an atomic ensemble. *Phys. Rev. Lett.* 107, 143005. doi:10.1103/physrevlett.107.143005

Schütz, S., Habibian, H., and Morigi, G. (2013). Cooling of atomic ensembles in optical cavities: semiclassical limit. *Phys. Rev. A* 88, 033427. doi:10.1103/physreva.88.033427

Schütz, S., Jäger, S. B., and Morigi, G. (2015). Thermodynamics and dynamics of atomic self-organization in an optical cavity. *Phys. Rev. A* 92, 063808. doi:10.1103/physreva.92.063808

Schütz, S., Jäger, S. B., and Morigi, G. (2016). Dissipation-assisted prethermalization in long-range interacting atomic ensembles. *Phys. Rev. Lett.* 117, 083001. doi:10.1103/physrevlett.117.083001

Schütz, S., and Morigi, G. (2014). Prethermalization of atoms due to photon-mediated long-range interactions. *Phys. Rev. Lett.* 113, 203002. doi:10.1103/physrevlett.113.203002

Stenholm, S. (1986). The semiclassical theory of laser cooling. *Rev. Mod. Phys.* 58, 699–739. doi:10.1103/revmodphys.58.699

Tishin, A., and Spichkin, Y. (2003). *The magnetocaloric effect and its applications*. 1st ed. Boca Raton: CRC Press.

Torggler, V., and Ritsch, H. (2014). Adaptive multifrequency light collection by self-ordered mobile scatterers in optical resonators. *Optica* 1, 336. doi:10.1364/optica.1.000336

Vinjanampathy, S., and Anders, J. (2016). Quantum thermodynamics. *Contemp. Phys.* 57, 545–579. doi:10.1080/00107514.2016.1201896

Vuletić, V., and Chu, S. (2000). Laser cooling of atoms, ions, or molecules by coherent scattering. *Phys. Rev. Lett.* 84, 3787–3790. doi:10.1103/physrevlett.84.3787

Wieman, C. E., Pritchard, D. E., and Wineland, D. J. (1999). Atom cooling, trapping, and quantum manipulation. *Rev. Mod. Phys.* 71, S253–S262. doi:10.1103/revmodphys.71.s253

Wineland, D. J., and Itano, W. M. (1979). Laser cooling of atoms. *Phys. Rev. A* 20, 1521–1540. doi:10.1103/physreva.20.1521

Wolke, M., Klinner, J., Keßler, H., and Hemmerich, A. (2012). Cavity cooling below the recoil limit. *Science* 337, 75–78. doi:10.1126/science.1219166

Wu, Z., Fan, J., Zhang, X., Qi, J., and Wu, H. (2023). Signatures of prethermalization in a quenched cavity-mediated long-range interacting fermi gas. *Phys. Rev. Lett.* 131, 243401. doi:10.1103/physrevlett.131.243401

Zhang, X., Chen, Y., Wu, Z., Wang, J., Fan, J., Deng, S., et al. (2021). Observation of a superradiant quantum phase transition in an intracavity degenerate fermi gas. *Science* 373, 1359–1362. doi:10.1126/science.abd4385